Positive and Negative Eddy Feedbacks Acting on Midlatitude Jet Variability in a Three-Level Quasigeostrophic Model

Loïc Robert, Gwendal Rivière, Francis Codron

Positive and Negative Eddy Feedbacks Acting on Midlatitude Jet Variability in a Three-Level Quasigeostrophic Model

LOÏC ROBERT AND GWENDAL RIVIÈRE

LMD/IPSL, Département de Géosciences, ENS, PSL Research University, École Polytechnique, Université Paris Saclay, Sorbonne Universités, UPMC Univ Paris 06, CNRS, Paris, France

FRANCIS CODRON

LOCEAN/IPSL, Sorbonne Universités, UPMC Univ Paris 06, CNRS, Paris, France

(Manuscript received 27 July 2016, in final form 15 February 2017)

ABSTRACT

The variability of midlatitude jets is investigated in a long-term integration of a dry three-level quasigeostrophic model on the sphere. As for most observed jets, the leading EOF of the zonal-mean wind corresponds to latitudinal shifts of the jet, and the second EOF to pulses of the jet speed. The first principal component (PC1) is also more persistent than the second one (PC2); this longer persistence arises from different eddy feedbacks both in the short term (i.e., within a few days following the peak of the PCs) and in the long term. The short-term eddy feedbacks come from two distinct mechanisms. First, a planetary waveguide effect acts as a negative feedback on both PCs. The positive phases of PC1 and PC2, which correspond to poleward-shifted and accelerated jets, respectively, are first driven then canceled by planetary waves reflecting on the equatorward flank of the jet. A similar process occurs for the negative phases when planetary waves reflect on the poleward flank of the jet. Second, synoptic waves also exert a short-term negative feedback on PC2: when the jet accelerates, the enhanced meridional wind shear increases the barotropic sink of eddy energy and depletes it very rapidly, therefore preventing synoptic eddies from maintaining the accelerated jet. Finally, at lags longer than their typical time scale, synoptic eddies drive a positive feedback on PC1 only. This feedback can be explained by a baroclinic mechanism in which the jet shift modifies the baroclinicity, causing, first, eddy heat flux anomalies and, then, momentum convergence anomalies. This feedback is absent for PC2, despite some changes in the baroclinicity.

1. Introduction

Midlatitude jets are also called eddy-driven jets because they are maintained against surface drag by the convergence of momentum by eddies (Vallis 2006). These eddies in turn develop in regions of strong baroclinicity, which tend to follow the jet position through thermal wind balance. The eddies and the jet are thus tightly coupled and how their interaction influences the variability of the jet is still not fully understood. The convergence of eddy momentum fluxes, herein called the eddy momentum forcing (Feldstein and Lee 1996; Lorenz and Hartmann 2001, hereafter LH01), drives fluctuations of the midlatitude jet but can also feedback on the jet anomalies in a way that increases their persistence (Gerber and Vallis 2007). Understanding these eddy feedbacks seems to be the key to explain the behavior of the jet (Zurita-Gotor et al. 2014; Lorenz 2014).

The observed low-frequency variability in the midlatitudes, whether given by EOFs of the geopotential height (annular modes; Thompson and Wallace 2000) or of the zonal-mean zonal wind (Gerber and Vallis 2007), is dominated by latitudinal shifts of the jets around their mean positions (Codron 2007; Vallis and Gerber 2008). The second EOF of the zonal-mean zonal wind, which represents an acceleration/deceleration of the jet at a rather constant latitude, explains less variance, especially at longer time scales (LH01; Lorenz and Hartmann 2003).

When looking at the scale of an oceanic basin, the picture becomes more complex but the variability remains generally dominated by jet shifts. In the North Atlantic, the leading wintertime EOF of the

Corresponding author e-mail: Loïc Robert, lrobert@lmd.ens.fr

DOI: 10.1175/JAS-D-16-0217.1

zonal-mean zonal wind, which is closely related to the North Atlantic Oscillation, mainly corresponds to a latitudinal shift of the jet (Eichelberger and Hartmann 2007; Vallis and Gerber 2008). In the North Pacific, the leading EOF of the zonal-mean zonal wind corresponds more to a pulsing of the jet (Eichelberger and Hartmann 2007) that is well correlated to the Pacific–North America (PNA) teleconnection pattern (Linkin and Nigam 2008), but the west Pacific pattern, which is the dominant mode in the western North Pacific, corresponds to a latitudinal shift of the jet (Linkin and Nigam 2008; Rivière 2010). In the Southern Hemisphere, the leading mode of variability is in most cases a latitudinal shift, but there are some exceptions such as the wintertime Pacific basin where there is a seesaw between two preferential jet positions (Codron 2007).

The dominance of jet shifts in most cases can be explained by their longer persistence compared to a jet acceleration or pulsing (Ring and Plumb 2008). This difference in persistence has been attributed to the existence of a positive eddy feedback acting on jet shifts only (LH01; Lorenz and Hartmann 2003; Yang and Chang 2007; Barnes and Hartmann 2011). The evidence for this positive feedback is seen in the cross correlation between time series of an index of the jet variability, such as the first principal component (PC), and of its forcing by eddy momentum fluxes. The correlation is significantly positive when the eddy forcing lags between a few days and a few weeks after the peak of the PC (LH01), corresponding to longer lags than the decorrelation time scale of the eddy forcing. LH01 has also shown that this positive feedback was mainly due to synoptic transient eddies. In cases when jet pulsing emerges as the leading mode, the positive synoptic eddy feedback acting on the shifting variability is usually very weak. It can happen for instance when the jet or the wave stirring region is close to the pole (Barnes and Hartmann 2011; Michel and Rivière 2014).

To understand its origin, this positive synoptic eddy feedback has been investigated using a wide range of models: barotropic quasigeostrophic models (Barnes and Hartmann 2011; Lorenz 2014), baroclinic quasigeostrophic models (Zhang et al. 2012), simplified dry GCMs (Gerber and Vallis 2007), aquaplanet GCMs with full physics (Michel and Rivière 2014), comprehensive atmospheric GCMs (Arakelian and Codron 2012; Simpson et al. 2013), and even coupled climate models (Arakelian and Codron 2012). Many dynamical mechanisms have been proposed, which can be divided into two main categories: barotropic and baroclinic. In the baroclinic mechanisms, the shifting of the jet is accompanied by a similar shift of the region of maximum baroclinicity and of wave sources. Eddies will then converge momentum to the new source region, maintaining the jet position. This shift of the baroclinic region can be induced by friction near the ground (Robinson 2000) or by a secondary circulation (Gerber and Vallis 2007). A complementary explanation has been proposed by Zhang et al. (2012): the baroclinicity consumed by synoptic waves can be restored by planetary waves. Barotropic mechanisms are based on changes in the horizontal propagation (and thus momentum transport) of waves, with no changes of the wave source. These changes can be due to the characteristics of the waves or to changes in the background mean state. In particular, the position of critical latitudes (Barnes and Hartmann 2011) or reflecting levels (Lorenz 2014) can affect the propagation of the synoptic waves and their breaking and, therefore, impact the deposition of momentum that drives the jet. These two kinds of feedback mechanisms are not exclusive and both may concurrently contribute to maintain jet shifts (Barnes and Thompson 2014; Zurita-Gotor et al. 2014).

If the positive eddy feedback can explain the longer persistence of jet shifts, its signature is only present after a certain period of time, usually beyond 5 days. Indeed, at shorter lags, the cross correlation with the eddy forcing is strongly negative, even for jet shifts, which is sometimes considered as resulting from a negative feedback due to planetary waves (Lorenz and Hartmann 2003; Simpson et al. 2013). This negative planetary wave feedback is not often discussed in the literature, but it is an important component of the eddy–mean flow interactions. Indeed, Simpson et al. (2013) showed that the lack of such a negative feedback in their model compared to the observed case explained the overestimated persistence of their leading EOF. A companion paper (Rivière et al. 2016, hereafter RRC16) studied the nature of this negative feedback by planetary waves in a three-level quasigeostrophic model on the sphere and showed that it was the signature of the reflection of waves on both sides of the jet. RRC16 focused on the mechanism of planetary wave reflection but did not investigate the leading modes of variability in the model, nor their persistence. The present paper aims to interpret the persistence of the leading modes of the jet variability in the same model and the roles of the different synoptic and planetary wave feedbacks. The main questions that are addressed are as follows:

- What is the nature of the leading mode of variability in the model?

- Is there a positive synoptic eddy feedback acting on the leading mode of variability? Is it of a barotropic or baroclinic nature?
- How important are the positive synoptic eddy feedback and negative planetary eddy feedback for the selection of the leading mode of variability?
- Do synoptic waves play a role in the long term only? What is their role in the short term?

After a description of the numerical model and the analyzed simulation in section 2, the two leading modes of variability of the jet are described in section 3. Short-term dynamics and feedback mechanisms are investigated for planetary and synoptic waves separately in section 4. Then, in section 5, the classical positive eddy feedback is discussed before ending by some concluding remarks in section 6.

2. Model

The model used is the dry quasigeostrophic model on the sphere described in Marshall and Molteni (1993), here at a T42 resolution. It has three pressure levels in the vertical at 200, 500, and 800 hPa. The model is governed by the following equations for the quasigeostrophic potential vorticity q_i at levels $i = 1, 2, 3$:

$$\frac{\partial q_i}{\partial t} + J(\psi_i, q_i) = S_i(\psi_{i-1}, \psi_i, \psi_{i+1}) - D_i(\psi_i),$$
$$q_i = f + \Delta\psi_i + \left(\frac{\psi_i - \psi_{i+1}}{R_i^2} - \frac{\psi_{i-1} - \psi_i}{R_{i-1}^2}\right), \tag{1}$$

where ψ_i is the streamfunction ($\psi_0 = \psi_1$ and $\psi_4 = \psi_3$), R_i is the deformation radius between levels i and $i + 1$, $S_i - D_i$ is the source and dissipative terms, and $f = 2\Omega\sin(\varphi)$ is the Coriolis parameter. The deformation radii are set to $R_1 = 660$ km and $R_2 = 400$ km as in Rivière (2009) and RRC16.

Source and dissipative terms are the sum of three distinct contributions. First, the forcing is implemented using Newtonian relaxation to a fixed profile (denoted with a tilde) using two different time scales $\tau_{R_1} = 40$ days and $\tau_{R_2} = 15$ days depending on the interface considered. Second, a scale-selective horizontal diffusion is applied at each level and tuned using the parameter c_H such as the damping time scale of the shorter waves at T42 truncation is 0.02 days. Finally, a linear drag with a time scale of $\tau_E = 3$ days is applied on the third (near surface) level. The complete source and dissipative terms are therefore given by

$$S_1 - D_1 = -c_H\nabla^8(q_1 - f) + \frac{1}{\tau_{R_1}}\frac{\psi_1 - \psi_2 - \tilde{\psi}_1 + \tilde{\psi}_2}{R_1^2},$$
$$S_2 - D_2 = -c_H\nabla^8(q_2 - f) - \frac{1}{\tau_{R_1}}\frac{\psi_1 - \psi_2 - \tilde{\psi}_1 + \tilde{\psi}_2}{R_1^2} + \frac{1}{\tau_{R_2}}\frac{\psi_2 - \psi_3 - \tilde{\psi}_2 + \tilde{\psi}_3}{R_2^2}, \quad \text{and}$$
$$S_3 - D_3 = -c_H\nabla^8(q_3 - f) - \frac{1}{\tau_{R_2}}\frac{\psi_2 - \psi_3 - \tilde{\psi}_2 + \tilde{\psi}_3}{R_2^2} - \frac{1}{\tau_E}\nabla^2\psi_3.$$

The potential vorticity is forced by a relaxation to a zonally symmetric temperature profile that is in thermal wind balance with a Gaussian zonal jet given by

$$\tilde{u}_i(\lambda, \varphi) = F_i U_0 \exp\left[-\frac{(\varphi - \varphi_0)^2}{d\varphi^2}\right],$$

where $U_0 = 50\,\mathrm{m\,s^{-1}}$, $\varphi_0 = 30°$N, and $d\varphi = 20°$ are the maximum intensity, mean position, and width of the jet and F_i is a baroclinicity factor set to $F_1 = 1$, $F_2 = 0.5$, and $F_3 = 0.2$.

The simulation is 15 yr long to ensure significant results and the first 350 days are discarded before the analysis. It is the same as the long-term simulation studied in RRC16.

3. Jet variability

The climatological jet (defined as the zonally and vertically averaged wind) is shown in Fig. 1a. It peaks around 46°N, shifted 16° poleward from the relaxation profile owing to the increased likelihood of anticyclonic wave breaking compared to cyclonic one in this model (Rivière 2009). The daily jet latitude, shown in blue, oscillates between 40° and 50°N. The two leading EOFs of the zonal- and vertical-mean wind are shown in Fig. 1b. On one hand, the first EOF, which explains 35% of the variance, has a node close to the climatological wind maximum and represents a shift of the jet. On the other hand, the second EOF, which explains 31% of the variance, reaches its maximum amplitude on the jet axis and, therefore, represents a strengthening of the jet, with a decrease in the subtropics.

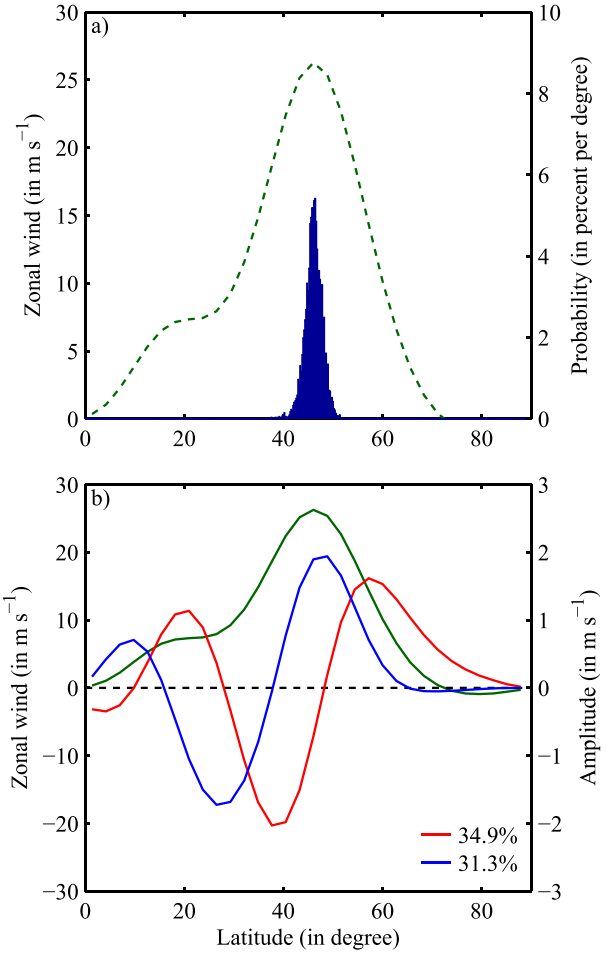

FIG. 1. (a) Time average of the zonal-mean zonal wind (dashed green line) and PDF of the daily positions of the maximum zonal-mean zonal wind (blue histogram) and (b) meridional structure of EOF1 (red) and EOF2 (blue) superimposed on the mean zonal wind profile (green). The vertical mean of the wind is used in each case. The percentages of variance explained are given for each EOF in the lower-right corner.

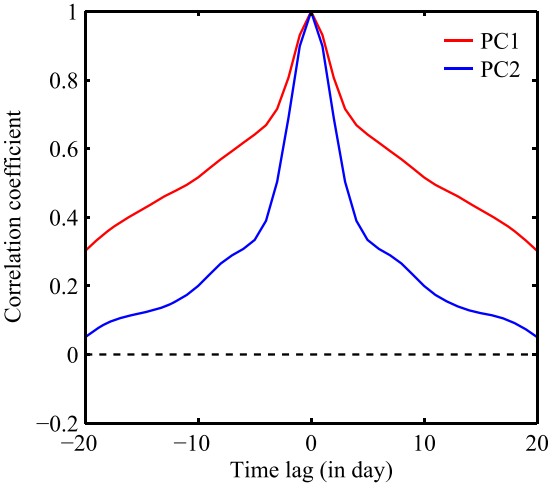

FIG. 2. Autocorrelation function of the principal component for EOF1 (red) and EOF2 (blue).

To estimate the persistence of each mode, the autocorrelation functions of the corresponding PCs are plotted in Fig. 2. Both curves share a similar shape: a fast decay rate in the first 4–5 days, followed by a slower one. This shoulder in the autocorrelation functions was also mentioned by Gerber and Vallis (2007) in their simulations of a dry primitive-equation model. In the following, we will therefore study separately the processes governing the evolution of the PCs at small and longer lags.

Jet shifts (PC1) have a smaller decay rate than jet pulses (PC2) both before and after the first 4–5 days, leading to a much larger persistence at longer lags. At lag +4 days, the autocorrelation decreases to 0.68 for PC1 and to 0.36 for PC2—namely, a factor of 2 between the two. From then on, the two autocorrelation curves are roughly parallel, meaning that the exponential decay rate is again slower for PC1 (if the decay rates of PC1 and PC2 were equal, the curves would tend to converge): the decay time scale after 5 days can be estimated at 24 days for PC1 and only 10 days for PC2.

To isolate the origins of the difference in persistence between the two PCs, the tendency equation for each PC is derived as in LH01 and other subsequent studies on the topic. The tendency equation for the vertical and zonal average of the zonal wind is first written as

$$\frac{\partial\langle[u]\rangle}{\partial t} = -\frac{1}{a\cos^2\varphi}\frac{\partial}{\partial\varphi}(\langle[u^*v^*]\rangle\cos^2\varphi) - \frac{[u_3]}{3\tau_E}, \quad (2)$$

where $\langle X\rangle$ and $[X]$ are the vertical and zonal means of X, respectively, and X^* is the deviation from the zonal mean. The first term on the rhs of Eq. (2) is the eddy momentum flux convergence and the second term is the linear surface drag. The scale-selective diffusion term is not written in this equation as it is negligible (not shown). The projection of Eq. (2) onto the structure of each EOF can be expressed as

$$\frac{\partial \mathrm{PC}}{\partial t} = m + d, \quad (3)$$

where m is the eddy momentum forcing (i.e., the projection of the eddy momentum flux convergence) and d is the projection of the surface drag. Surface drag, which is proportional to the projection of $[u_3]$ onto each EOF, is therefore not exactly proportional to the PC in contrast with the simple barotropic model in LH01.

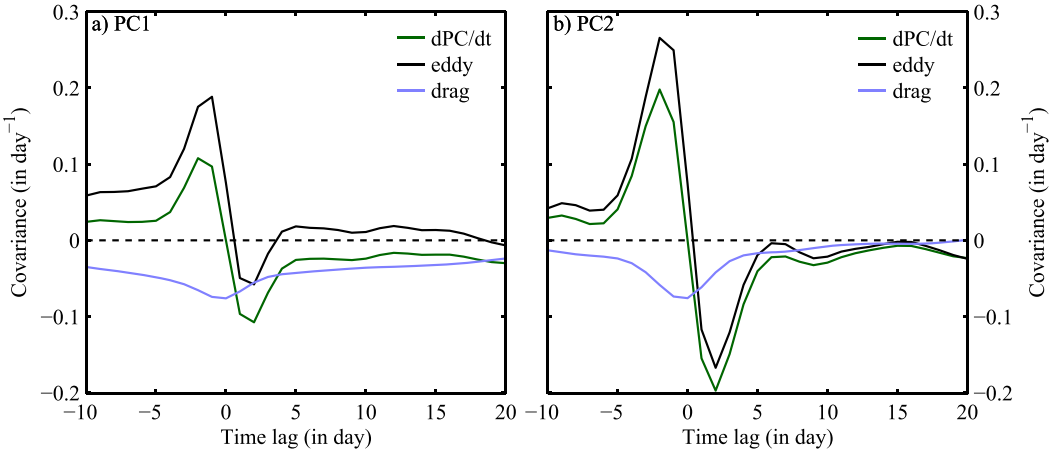

FIG. 3. Cross covariances between each PC and its time derivative (green), eddy forcing (black), and surface drag (light purple) for (a) PC1 and (b) PC2. Because PC is nondimensional, these quantities are plotted in units of day^{-1}. The PC leads for positive lags.

The cross covariance between the PCs and each of the three terms of Eq. (3) is plotted in Fig. 3. The cross covariance between a PC and its time derivative is equal to the derivative of the PC autocorrelation function, so the two cross-covariance functions with m and d can be directly interpreted as the components of the PC autocorrelation tendency due to the eddy momentum forcing and the drag, respectively.

The linear drag term is more or less proportional to the PC itself, even though it acts only on the surface wind. At negative lags, the zonal wind anomalies are forced by eddies. The cross covariance of this forcing is 50% larger for PC2. This stronger eddy forcing of PC2 is compensated by its shorter persistence relative to PC1 and explains why the two PCs are close in terms of total variance. At short positive lags, the eddy forcing becomes negative, explaining the fast decay rate. This negative tendency is present for both PCs but is about 4 times stronger for PC2.

In the longer term, the eddy forcing cross covariance is significantly positive for PC1 between lags +5 and +15 days, which is the typical signature of a positive eddy feedback according to some previous studies (LH01; Zurita-Gotor et al. 2014). For PC2, however, this cross covariance is close to zero or slightly negative.

In summary, the difference in persistence between the two leading modes of variability can be analyzed at two distinct time scales:

- In the short term, between lags 0 and +4 days, the PCs autocorrelation functions decrease rapidly because of a negative cross covariance with the eddy forcing. Section 4 will be devoted to linking this negative cross covariance to planetary and synoptic feedback mechanisms.
- In the long term, beyond lag +5 days, a positive cross covariance with the eddy forcing is observed for PC1 only. This long-term positive tendency is studied in section 5 and is shown to correspond to a positive feedback consistent with LH01 and Zurita-Gotor et al. (2014).

4. Short-term feedback

a. Planetary and synoptic components

As shown in previous studies, the feedback of eddies on the jet can strongly depend on their zonal wavenumber k (Zhang et al. 2012; Simpson et al. 2013; RRC16). We therefore separate them into two distinct ranges: planetary waves ($k \in [1, 4]$) and synoptic waves ($k \geq 5$). The reason for the choice of wavenumbers is shown in Fig. 4: while synoptic waves deposit their momentum very close to the jet axis, planetary waves do it on the jet flanks as already shown in O'Rourke and Vallis (2013, 2016). This can be attributed to distinct regions of excitation: because synoptic waves have higher phase speed, their critical lines (i.e., where the phase speed equals the background zonal wind) are closer to the jet core than for planetary waves. Since waves more easily tap the baroclinicity where critical lines appear, the regions of excitation and momentum deposition will also differ between synoptic and planetary waves (Zhang et al. 2012). Another mechanism in the planetary case is the wave reflection on the jet flanks, as documented in RRC16.

The eddy momentum forcing can be exactly decomposed into the sum of a planetary component p and a synoptic component s:

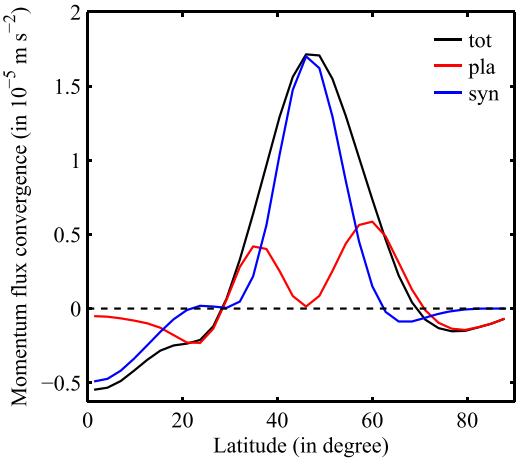

FIG. 4. Climatological mean of the vertically integrated eddy momentum flux convergence (black) and its planetary (red) and synoptic (blue) components.

$$[u^*v^*] = [u_p^*v_p^*] + [u_s^*v_s^*] \Rightarrow m = m_p + m_s.$$

The cross covariance between each PC and the total, planetary, and synoptic eddy forcings are plotted in Fig. 5. In all cases, the covariance is positive when eddies lead, meaning that both types of waves contribute to forcing the jet variability. The picture becomes more complex at short positive lags. The planetary eddy forcing exhibits a negative cross covariance with both PC1 and PC2 that is slightly stronger with PC2. The synoptic eddy forcing also has a negative cross covariance with PC2, but the cross covariance with PC1 is slightly positive, implying distinct synoptic wave dynamics for the two PCs. The following subsections are devoted to showing that these cross-covariance short-term tendencies can be related to various types of eddy feedbacks.

b. Planetary feedback

As shown in Fig. 5, the short-term cross covariance between the PC and the planetary eddy forcing behaves similarly for PC1 and PC2. To understand its dynamical origin, composites of the total planetary momentum flux and its associated anomalous convergence are shown in Fig. 6 for both phases of PC2. Composites for the positive (negative) phase are calculated based on days t when PC2(t) is both greater than 1.5 (smaller than −1.5) standard deviation and a local maximum (minimum) on the interval $[t-2, t+2]$. This corresponds to 112 events for the positive phase and 106 events for the negative phase.

For the negative phase (Fig. 6a), which corresponds to a weaker and wider jet, momentum flux divergence occurs in the jet core before lag 0 together with a momentum flux convergence on its equatorward flank. This tends to weaken and widen the jet and correspond to the strong positive cross covariance at negative lags in Fig. 5b. But at positive lags, the convergence pattern changes sign, resulting in a strong negative cross covariance and tends to cancel out its previous impact on the jet. The same phenomenon happens for the positive phase (Fig. 6b) because the momentum flux convergence pattern has opposite signs. The strengthening and sharpening of the jet at negative lags is followed by the counter effect at positive lag. Composites for PC1 (not shown) also display very similar patterns but slightly weaker and centered on the jet axis. The anomalous dipole in momentum convergence tends to shift the jet poleward for the positive phase and equatorward for the

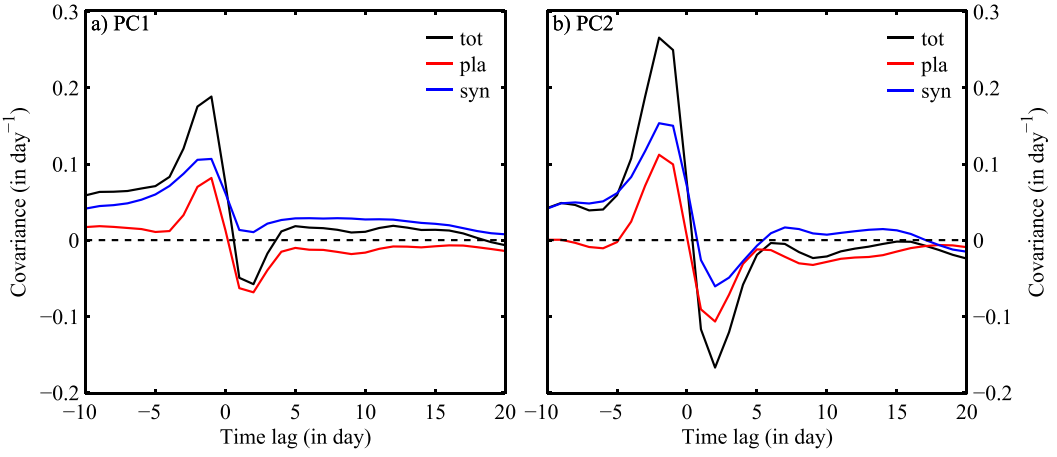

FIG. 5. Cross covariances between each PC and its total eddy forcing (black), and the planetary (red) and synoptic (blue) components for (a) PC1 and (b) PC2. PC leads for positive lags.

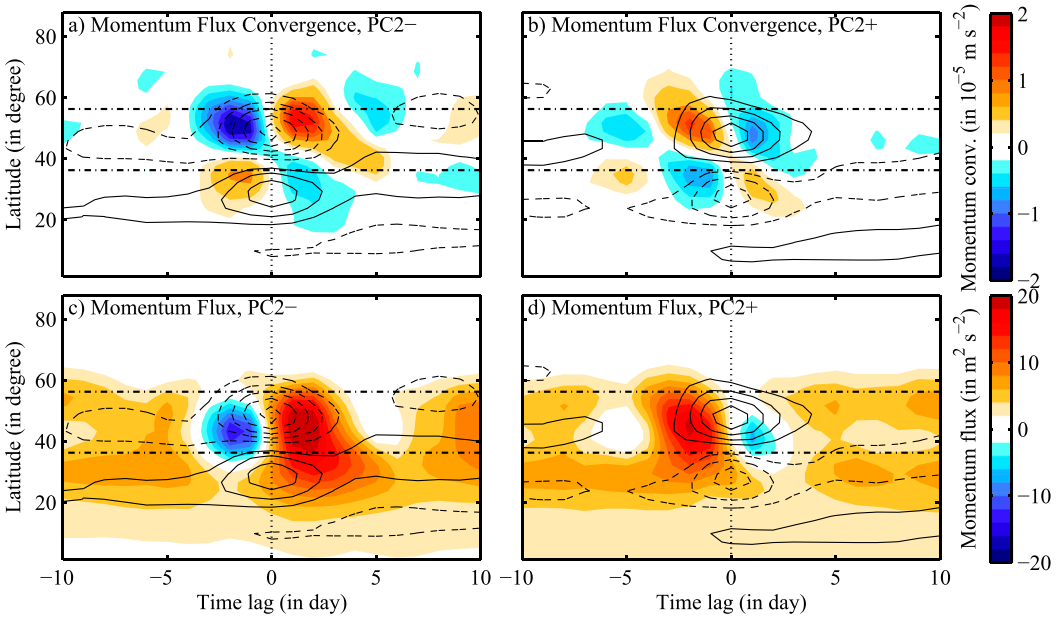

FIG. 6. In shading, lagged composites for (left) negative and (right) positive phases of PC2: (a),(b) planetary momentum flux convergence anomaly and (c),(d) planetary momentum flux. Composites of the corresponding zonal wind anomalies are superimposed (contour interval: 0.5 m s^{-1}). Negative contours are dashed and the zero contour is omitted. The dotted line indicates lag 0 and the dashed–dotted lines are the meridional extension of the mean jet (which corresponds to ±10° around the jet axis).

negative phase at short negative lags but then cancels out this effect because of an abrupt change in sign at short positive lags.

To understand the evolution of momentum flux convergence, composites of momentum fluxes have been plotted in Figs. 6c and 6d for both phases. For the negative phase (Fig. 6c), momentum fluxes are negative before lag 0 and centered equatorward of the jet core, which can explain the convergence pattern observed in Fig. 6a. This negative momentum flux at negative lags is followed by a positive momentum flux at positive lags. Since the group velocity of Rossby waves and their associated momentum flux have opposite sign, a sudden change in the sign of the momentum flux suggests that waves are reflected. Figures 6c and 6d therefore suggest that waves propagate poleward and then equatorward during the negative phase whereas the opposite occurs during the positive phase. This hypothesis is supported by RRC16 results.

A schematic depiction is shown in Fig. 7 to summarize the main findings of RRC16 in the context of a pulsing event. Dipoles of momentum flux convergence with opposite signs for negative and positive time lags are represented in Fig. 7a (Fig. 7b) as in Fig. 6c (Fig. 6d). Wave reflection on the poleward flank of the jet can frequently occur because of the quasi-permanent presence of a turning latitude (i.e., a latitude where the refractive index n equals zero). This quasi-permanent turning latitude is shown by the thick black line in Fig. 7a. The reflection leads to the transient forcing then damping of a negative phase (cf. Fig. 7a and Figs. 6a,c). On the equatorward flank of the jet, wave reflection is less systematic but may happen if the PV is well homogenized in the subtropical critical layer during the equatorward propagation of the wave. In Fig. 7b, this transient turning latitude is shown by the short thick line around day 0 when the reflection happens. It would force then damp a positive phase (Figs. 7b and 6b,d). Note that the waveguide is not centered on the jet axis but is shifted to its equatorward side because of the spherical geometry (see RRC16 for more details).

To conclude, planetary waves are shown to both force jet fluctuations and cause a short-term negative feedback when they are reflected. This feedback explains an important part of the negative cross covariance at small positive lags observed for both PCs (Fig. 5). The planetary wave reflection mechanism can also explain why the negative cross covariance between the PC and the planetary momentum forcing is a bit stronger for PC2. Indeed, the equatorward shift of the waveguide can lead to a better projection of the planetary momentum flux convergence onto EOF2 than onto EOF1, as described in RRC16. Moreover, contrary to a shifting of the jet, a pulsing event tend to modify the PV gradient profile,

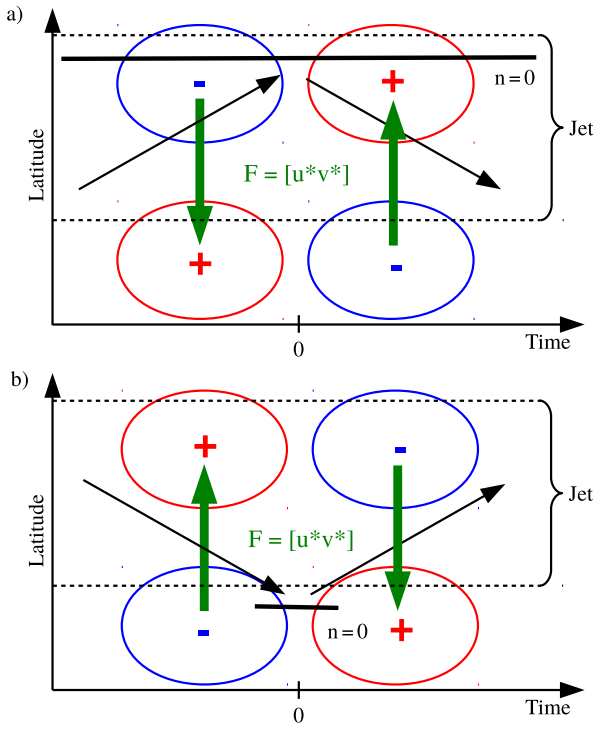

FIG. 7. Schematic depiction of the sequence of planetary wave forcing onto the jet and planetary wave reflection during (a) negative and (b) positive phases of PC2. The black arrows indicate the direction of propagation of the planetary wave and the thick solid line is the reflecting level ($n = 0$), with time increasing to the right. The horizontal dashed lines indicate the meridional extension of the jet. The green arrows show the momentum fluxes associated with the wave propagation, and the induced convergence and divergence of momentum flux are drawn in red and blue, respectively. Lag 0 corresponds to the day the reflection occurs.

making it stronger over the jet core but smaller in the subtropical region, which increases the likelihood of a transient turning latitude to form. But the difference in planetary negative feedback in Fig. 5 is too small to explain the total eddy forcing difference. The synoptic component must be taken into account as well.

c. *Synoptic feedback*

The nature of the short-term synoptic cross-covariance tendency significantly differs from the planetary waves case. First, it is strongly negative for PC2 and weakly positive for PC1 as shown in Fig. 5. Second, as shown by RRC16, the reflection of synoptic waves is very unlikely and is thus not a good candidate to explain this negative tendency. It seems instead to obey a different mechanism based on eddy kinetic energy.

The eddies and the zonal-mean flow can exchange energy through barotropic and baroclinic processes. Ignoring the diabatic terms and the meridional advection, the time derivative of the eddy total energy (ETE) can be written as the sum of a barotropic and a baroclinic conversion rate (Lorenz 1955; Rivière et al. 2013). Its formulation in the present quasigeostrophic framework is

$$\frac{\partial \mathrm{ETE}}{\partial t} = C_{\mathrm{bt}} + C_{\mathrm{bc}}, \tag{4}$$

where

$$\mathrm{ETE}(\varphi, t) = \sum_{i=1}^{3}\left[\frac{(u_i^*)^2 + (v_i^*)^2}{2}\right] + \sum_{i=1}^{2}\left[\frac{(T_i^*)^2}{2}\right], \tag{5}$$

$$C_{\mathrm{bt}}(\varphi, t) = -\sum_{i=1}^{3}[u_i^* v_i^*]\left(\frac{\partial [u_i]}{\partial y} + \frac{[u_i]\tan\varphi}{a}\right), \quad \text{and} \tag{6}$$

$$C_{\mathrm{bc}}(\varphi, t) = -\sum_{i=1}^{2}\left[\left(\frac{v_i^* + v_{i+1}^*}{2}\right)T_i^*\right]\frac{\partial [T_i]}{\partial y}, \tag{7}$$

where a is Earth's radius and $T_i = (\psi_i - \psi_{i+1})/R_i$ is a variable proportional to the temperature. Quantities involving the deviation from the zonal mean include both planetary and synoptic eddy components. From now on, we only focus on the synoptic eddy total energy and the interaction between the zonal-mean flow and the synoptic eddies. Hence, in the following computation of Eqs. (5)–(7), only the synoptic component of the eddies are taken into account in the deviation from the zonal mean. Even though the interaction between synoptic and planetary eddies may play a role in the evolution of synoptic eddy energy, it is not considered in the following discussion for the sake of simplicity.

As shown in Fig. 4, synoptic eddies mostly converge momentum into the jet core. Their effect onto the variations of the jet intensity could therefore be closely dependent on their amount of energy: more (less) synoptic eddy energy than usual would cause more (less) convergence of momentum flux into the jet core, which effect would be to accelerate (decelerate) the jet. This is confirmed when looking at the composite of synoptic ETE for the positive phase of PC2 (Fig. 8a) and comparing with the cross covariance of the synoptic forcing with PC2 (blue curve in Fig. 5b). Indeed, the maximum and minimum of the cross covariance at lags −2 days and +2 days correspond to more and less synoptic ETE than usual, respectively. Therefore, to better understand the negative minimum of the cross covariance at short positive lags, one should explain the deficit in synoptic ETE at those lags.

There are two hypotheses to explain this deficit. One is discussed in LH01 and Yang and Chang (2007) and refers to the "barotropic governor" mechanism. It is based on the results from James (1987) showing that

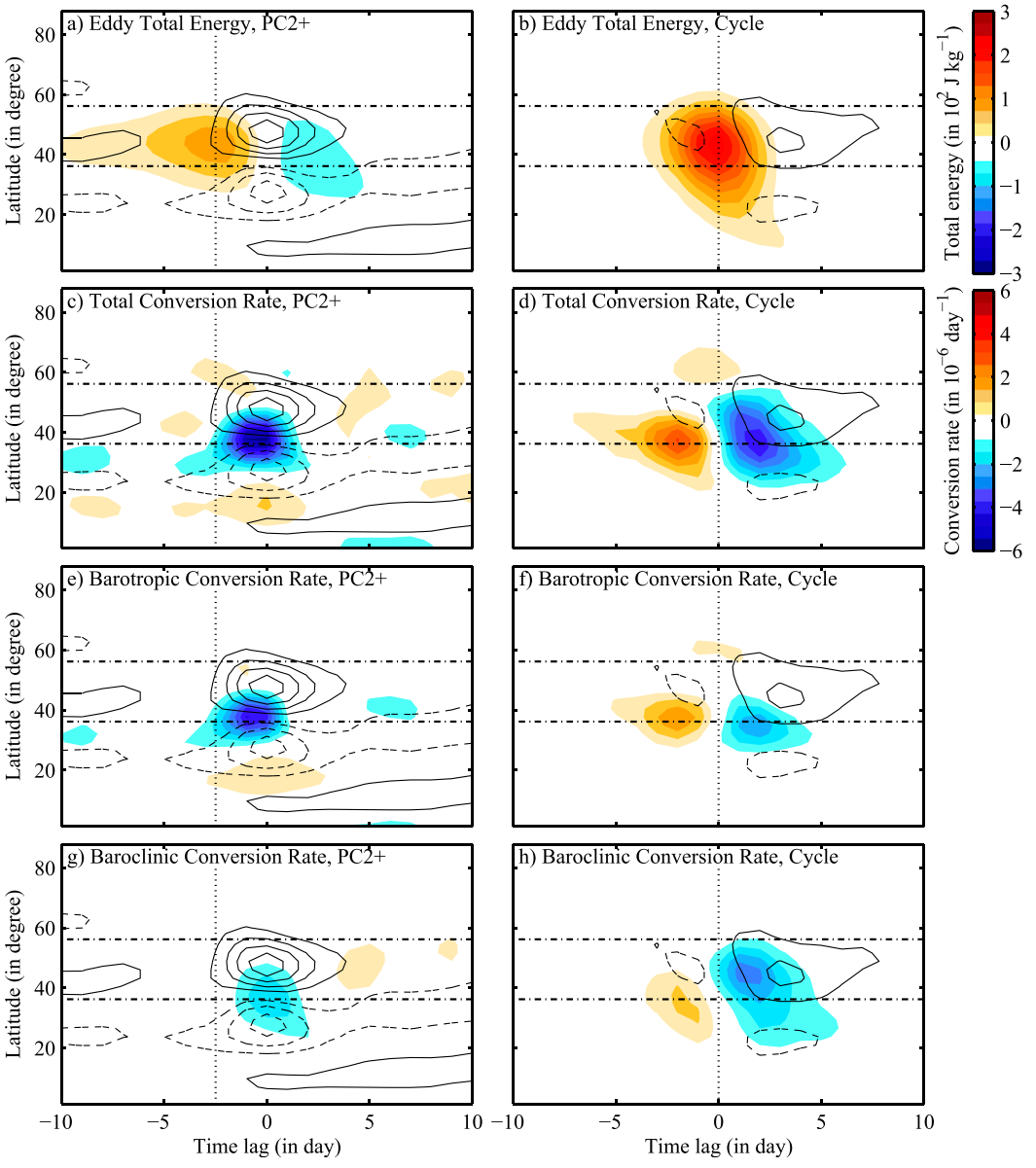

FIG. 8. In shading, lagged composites for (left) positive phase of PC2 and (right) the synoptic eddy life cycle: (a),(b) synoptic wave energy anomaly, (c),(d) total conversion rate anomaly, (e),(f) barotropic conversion rate anomaly, and (g),(h) baroclinic conversion rate anomaly. Composites of the corresponding zonal wind anomalies are superimposed (contours) as in Fig. 6. The dotted line indicates the lag of maximum energy anomalies and the dashed–dotted lines indicate the mean jet meridional extension (defined as in Fig. 6).

when the barotropic lateral shears of a baroclinic jet increase—as in the positive phase of PC2—there is a reduction in baroclinic wave growth. Another hypothesis is based on the idea that the increased shear induces a stronger barotropic decay of energy, because the barotropic conversion C_{bt} is directly dependent on the lateral shears [see Eq. (6)]. To test these two hypotheses, Eq. (4) is divided by ETE to compare the baroclinic exponential conversion rate $\sigma_{bc} = C_{bc}/\mathrm{ETE}$, the barotropic exponential conversion rate $\sigma_{bt} = C_{bt}/\mathrm{ETE}$, and the sum $\sigma = \sigma_{bt} + \sigma_{bc}$ (see Figs. 8g, 8e, and 8c, respectively). The rapid decrease in synoptic ETE occurring around lag 0 can be explained by a negative extrema of the anomalous total conversion rate (Fig. 8c). It is due to the stronger than usual barotropic decay (Fig. 8e) and, albeit to a lesser extent, to the weaker baroclinic growth than usual (Fig. 8g).

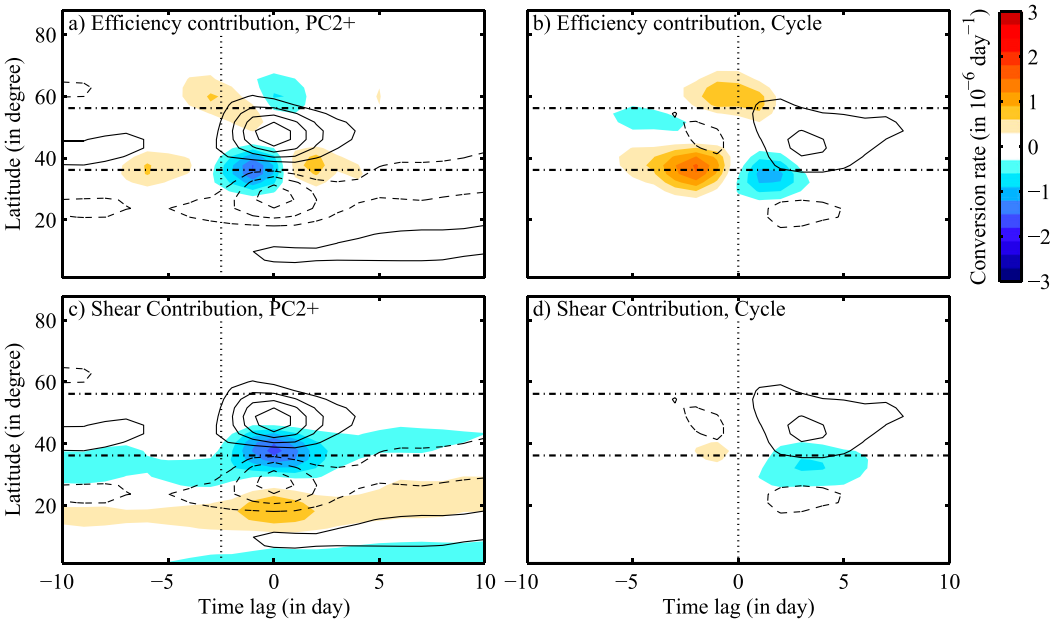

FIG. 9. As in Fig. 8, but for components of the barotropic conversion rate anomaly due to (a),(b) variations in the efficiency of waves in exchanging energy with the mean flow and (c),(d) variations in lateral shear.

It is important to understand whether this stronger barotropic sink of energy is a response to the jet acceleration or simply a signature of a classical baroclinic wave life cycle with baroclinic growth followed by barotropic decay (Simmons and Hoskins 1978). Following Moon and Feldstein (2009), this life cycle is obtained using meridionally averaged synoptic ETE as an index. To compare the behavior of synoptic eddies during the positive phase of PC2 with a typical baroclinic life cycle, composites of the same quantities are shown in the right column of Fig. 8. These composites are computed based on days when the index is greater than 1.5 standard deviations and is a local maximum, as for the PC2. As shown in Fig. 8b, positive anomalies of synoptic ETE, which maximum is by construction reached at the lag 0, seem to accelerate the jet, which confirms our previous assumption. However, this acceleration is weaker than in Fig. 8a because planetary waves also concur to a pulsing event. Besides, the decrease of ETE anomalies are driven by both the barotropic and baroclinic conversion rates, the baroclinic one being larger (see Figs. 8d,f,h). This differs from the PC2 case, in which the barotropic decay anomalies are more than twice as strong as the baroclinic ones and dominate the decrease in ETE. Therefore, the evolution of synoptic ETE during the positive phase of PC2 differs from a baroclinic life cycle, mainly through an increase in the rate of barotropic decay but not through a smaller baroclinic growth.

The stronger anomalies of σ_{bt} for PC2 are caused by anomalies in the lateral shear. To show this, a barotropic efficiency E_{bt} can be defined by rewriting σ_{bt} as follows:

$$\sigma_{\mathrm{bt}} = \frac{C_{\mathrm{bt}}}{\mathrm{ETE}} = E_{\mathrm{bt}}\left(\frac{\partial[u_i]}{\partial y} + \frac{[u_i]\tan\varphi}{a}\right) = E_{\mathrm{bt}}\mathrm{Sh},$$

where Sh is the zonal wind shear within the spherical framework. The barotropic efficiency depends on the wave structure but not on its amplitude. It characterizes, for a given wave, the efficiency of the exchange of energy with the mean flow for a given shear. To first order, the deviation of σ_{bt} from its time mean can be expressed as

$$(E_{\mathrm{bt}}\mathrm{Sh})' \simeq E'_{\mathrm{bt}}\overline{\mathrm{Sh}} + \overline{E}_{\mathrm{bt}}\mathrm{Sh}',$$

where bars and primes denote the time mean and the deviation from the time mean, respectively. The first and second terms on the right-hand side correspond to a change in efficiency with a constant shear and to a change in shear with a constant efficiency respectively. The residual was verified to be very small.

Lagged composites of these two components of σ_{bt} are shown in Fig. 9 together with the associated wind anomalies, again for the PC2 positive phase and for the life cycle. The component due to shear changes is much more important for PC2 than for the life cycle, because the wind anomalies are much more intense for the former (Figs. 9c,d). The component due to changes in

efficiency is of comparable amplitude in both cases, only a bit smaller for PC2 (cf. lag 0 of Fig. 9a with lag +2 days of Fig. 9b). Therefore, the stronger lateral shears are the main cause of the rapid decrease of the ETE after an acceleration of the jet, leading to the negative anomalies observed in Fig. 8a.

In summary, the short-term negative cross covariance observed for the synoptic eddy forcing of PC2 (see Fig. 5) has been shown to be the signature of a negative eddy feedback: the increased shear when the jet is accelerated increases the barotropic decay of the eddy energy and depletes the synoptic ETE faster than in a normal life cycle. The synoptic waves rapidly reach amplitudes below their climatological value and deposit less momentum into the jet core. This feedback mechanism is specific to PC2, as the lateral shears do not change in amplitude for latitudinal shifts of the jet. Finally, the barotropic governor mechanism has been discarded here because the stronger lateral shears during the positive phase of PC2 do not lead to smaller σ_{bc} compared to the typical life cycle (Figs. 8g,h).

5. Long-term feedback

In this section, we focus on the positive cross-covariance tendency between lags +5 and +15 days for PC1 (Fig. 3a) and its absence for PC2. As shown in Fig. 5, and in accordance with the literature (LH01; Lorenz and Hartmann 2003; Simpson et al. 2013), this tendency involves synoptic waves and not planetary waves whose momentum forcing is not correlated with PCs at these time scales. The aim of this section is to confirm that a feedback mechanism is at play and discriminate between barotropic or baroclinic feedback mechanisms to explain this long-term tendency.

To investigate the nature of the long-term feedback, the anomalous synoptic eddy momentum forcing at the upper level can be related to the synoptic heat flux entering this level through the divergence of the (synoptic) Eliassen–Palm flux (EP):

$$-\frac{1}{a\cos^2\varphi}\frac{\partial}{\partial\varphi}([u_1^*v_1^*]\cos^2\varphi)=\frac{[v_1^*T_1^*]}{R_1}+[q_1^*v_1^*]. \quad (8)$$

The first term on the rhs of Eq. (8) is the vertical divergence of the EP flux (i.e., the vertical convergence of the heat flux in the upper level) and the second term is the full EP flux divergence. These two terms can be interpreted respectively as the baroclinic and barotropic contributions to the eddy forcing. Indeed, if the heat flux (baroclinic) term dominates, it means that all the momentum flux convergence can be explained by anomalous wave activity entering the upper troposphere. On the contrary, a small heat flux term means that the anomalous momentum fluxes result from changes in wave propagation (i.e., barotropic mechanism), without any contribution from wave sources.

However, considering the total convergence of heat flux would overestimate the baroclinic contribution because not all the incoming waves radiate away from the jet owing to local dissipation of wave activity at the latitude of wave generation. It is thus necessary to estimate the amount of waves that are horizontally radiated. To estimate this radiation efficiency E, the ratio between the climatological convergences of momentum and heat flux at the upper level is averaged over the jet core (considered as ±10° around the jet maximum). This efficiency corresponds to the proportion of waves incoming from the lower levels that effectively radiate away from the jet core at the upper level. This proportion can vary between 0 (all incoming waves are trapped into the jet and no horizontal momentum transport occurs, as shown in Fig. 10a) and 1 (all incoming waves radiate away and produce momentum flux convergence into the jet core, as shown in Fig. 10b). In the former case, the divergence of the EP flux is equal to the vertical convergence of heat flux, while in the latter case, the horizontal and vertical components of the EP flux divergence cancel each other near the jet core. The remaining $(1-E)$ should be counted as barotropic contribution because it quantifies the local dissipation of baroclinic wave activity. Therefore, Eq. (8) can be rewritten as follows:

$$-\frac{1}{a\cos^2\varphi}\frac{\partial}{\partial\varphi}([u_1^*v_1^*]\cos^2\varphi) = E\frac{[v_1^*T_1^*]}{R_1}+\left\{(1-E)\frac{[v_1^*T_1^*]}{R_1}+[q_1^*v_1^*]\right\}. \quad (9)$$

In this simulation, E at the upper level is found to be equal to 80%.

The projection of each term of Eq. (9) on a given EOF is

$$\mathrm{MFC}=\mathrm{BC}+\mathrm{BT}, \quad (10)$$

where MFC is the total synoptic eddy momentum forcing at the upper levels and BC and BT can be seen as the respective contributions of baroclinic and barotropic feedbacks. The feedback is said to be barotropic when the feedback loop does not depend on changes in wave sources, which corresponds to the case when BC = 0 (i.e., when there is no correlation between the upper-level heat flux anomalies and the EOF). Indeed, in that case, the projection of the momentum convergence onto the EOF does not depend on the anomalous wave activity

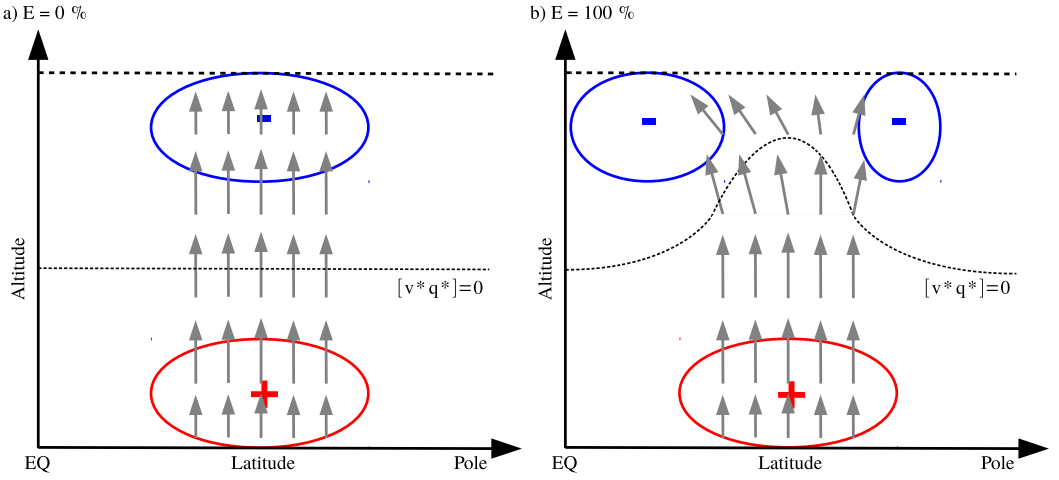

FIG. 10. Schematic depiction of Eliassen–Palm flux (gray arrows) and its resulting convergence (blue) and divergence (red) for different radiation efficiency: (a) $E = 0\%$ and (b) $E = 100\%$. The dashed line indicates where the divergence is null.

coming from lower levels and the feedback is thus barotropic. In contrast, when BT = 0, the effect of the horizontal divergence of the EP flux on the zonal-mean flow anomalies equals that of the vertical convergence of the EP flux and the feedback is said to be baroclinic. Figure 11 shows the cross covariance of these projections with the corresponding PCs. In both cases, the cross covariance of MFC is very similar to the vertically averaged one (Fig. 5), which is not surprising as most of the momentum fluxes is in the upper troposphere. For PC1 (Fig. 11a), between lags +4 days and +20 days, the barotropic term is weakly negative, whereas the baroclinic term is positive and almost equal to the total eddy momentum forcing. Hence, the long-term positive tendency is driven by baroclinic processes, similarly to the β-plane simulations of Zurita-Gotor et al. (2014). For PC2, a positive tendency at long terms also exists but is weaker (Fig. 11b).

To better characterize the underlying baroclinic processes and to assess if it is associated with a feedback mechanism, lagged composites of the baroclinicity, synoptic eddy heat flux, and zonal wind anomalies are shown for the positive phase of PC1 and PC2 in Fig. 12. The baroclinicity and heat flux anomalies are more persistent for PC1 than PC2. The baroclinicity anomalies tend to follow the zonal wind anomalies, with a shorter persistence for both anomalies in the case of PC2. The baroclinicity anomalies reach their maximum amplitude at lag +1 day. This slight lead of the zonal wind anomalies over the baroclinicity anomalies

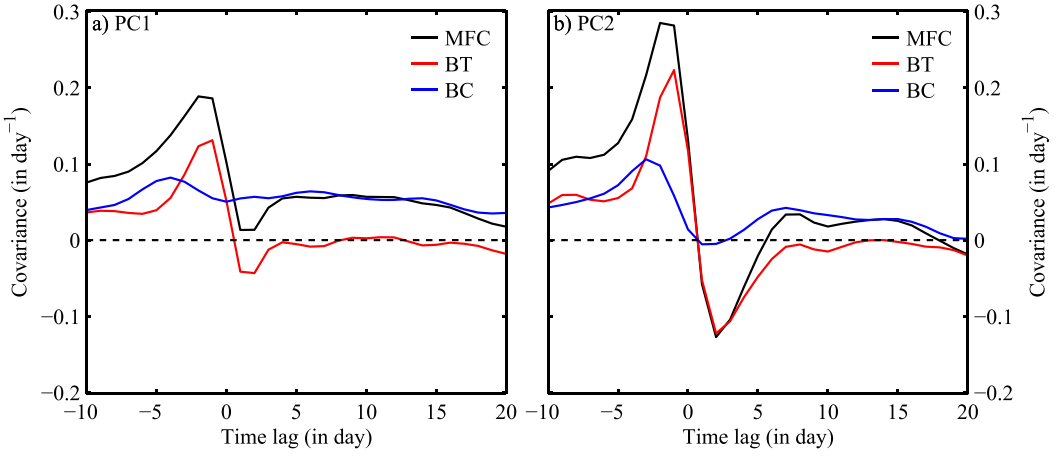

FIG. 11. Cross covariance between each PC and the corresponding synoptic eddy forcing (black, MFC) and its barotropic (red, BT) and baroclinic (blue, BC) contributions for (a) PC1 and (b) PC2, as defined in Eq. (10).

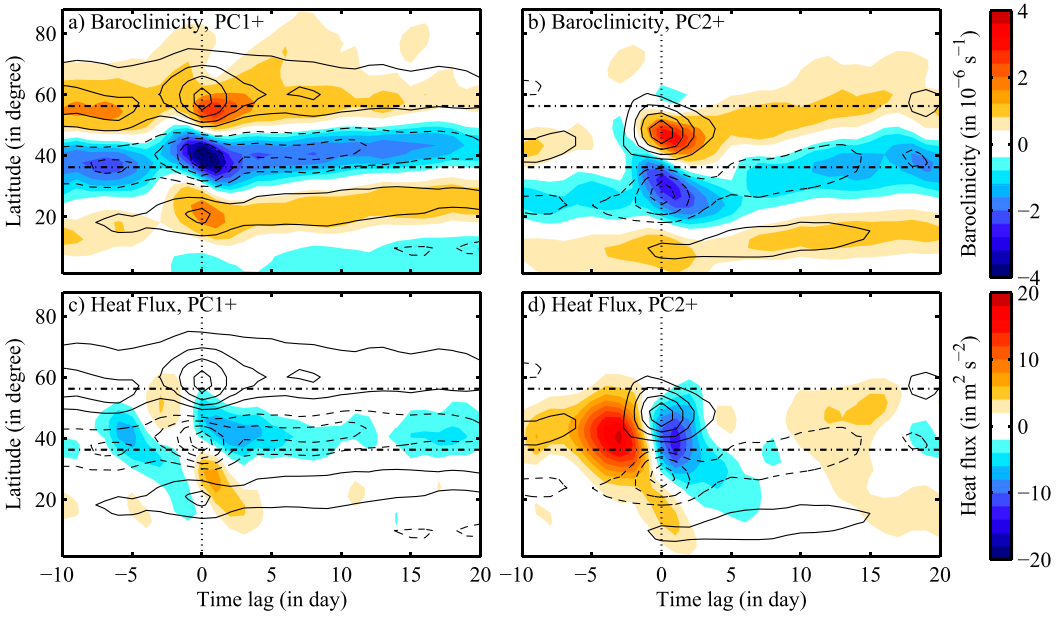

FIG. 12. In shading, lagged composites for the positive phase of (left) PC1 and (right) PC2: (a),(b) vertically averaged baroclinicity anomaly and (c),(d) synoptic heat flux anomaly at the interface between levels 2 and 3 (near surface). Composites of the corresponding zonal wind anomalies are superimposed (contours) as in Fig. 6. The dotted line indicates lag 0 and the dashed–dotted lines indicate the meridional extension of the mean jet (defined as in Fig. 6).

supports Robinson (2000)'s arguments whereby a barotropic modification of the jet triggers a similar change in baroclinicity because of the action of the friction at lower levels.

The link between the baroclinicity (or wind) and heat flux anomalies is not so obvious and strongly depends on the PC. They are well correlated for PC1, especially the negative anomalies on the equatorward side of the jet (Figs. 12a,c). They are however very different for PC2 (Figs. 12b,d). For instance, at short positive lags, strong negative heat flux anomalies appear in regions with both stronger and weaker baroclinicity than the climatological mean. These short-term negative heat flux anomalies are rather due to a global decrease in synoptic eddy energy because of the strong barotropic sink of energy (see section 4). At longer lags, the heat flux and wind anomaly are also uncorrelated.

The long-term positive cross covariance between the eddy forcing and PC1 observed in the model can be considered as resulting from a baroclinic feedback mechanism: the latitudinal shifts in the jet are followed by latitudinal shifts of the baroclinicity, which cause heat flux anomalies at low levels. These anomalies in the latitude of wave stirring explain those in the momentum flux convergence at upper levels which help to maintain the initial shift of the jet. This feedback only occurs for EOF1 and helps to increase the difference in persistence between the two leading modes of variability.

6. Conclusions

In the present study, the variability of a midlatitude jet has been studied in a long-term integration of a dry three-level quasigeostrophic model on the sphere forced by a relaxation in temperature toward a zonally symmetric profile. The dominant variability of the simulated jet is similar to the one of most observed jets: the leading EOF corresponds to a latitudinal shifting of the jet, the second EOF to a pulsing of the jet intensity, and PC1 is much more persistent than PC2. A positive feedback by synoptic eddies is acting on the first PC beyond a few days, as in observed jets (LH01; Lorenz and Hartmann 2003) and in other similar numerical experiments (Gerber and Vallis 2007; Zurita-Gotor et al. 2014), but the difference in persistence between the first two PCs is also due to short-term dynamics that are rarely discussed in the literature.

In the short term (i.e., within a few days after a peak in a PC), planetary waves exert a negative feedback onto the first two PCs owing to their reflections on the poleward or equatorward sides of the jet. The poleward shift in the jet and its acceleration, which correspond to the

positive phases of PC1 and PC2, respectively, can be driven by an equatorward propagation of planetary waves. The waves that are reflected on the equatorward flank of the jet, then feedback negatively onto the jet anomalies during their poleward propagation (see Fig. 7). A similar negative feedback occurs for the equatorward shift and deceleration of the jet (i.e., the negative phases of PC1 and PC2, respectively) when the planetary waves reflect on the poleward side of the jet. The reader is referred to the companion paper (RRC16) for further investigation about these reflections by planetary eddies.

In the short term again, synoptic waves also exert a negative feedback on PC2 but not on PC1, and its origin is very different from the planetary wave feedback. When the jet is accelerated (positive phase of PC2), horizontal wind shears are increased and the rate of decay of eddy kinetic energy by barotropic conversion becomes more strongly negative than for a standard baroclinic life cycle. This causes an abrupt depletion of the total energy of synoptic eddies, which decreases below its climatological mean just after the maximum intensity of the jet. The synoptic eddies, having less energy than usual, deposit less momentum into the jet core, which decelerate the jet and create the negative feedback. The negative phase of PC2 behaves as a mirror process: when the jet reaches its minimum amplitude, the wind shear is weaker, reducing the barotropic sink of synoptic eddy energy. This leads to a rapid increase in synoptic eddy energy and eventually a jet acceleration. Note that the baroclinic conversion rate does not change much between the different phases of PC2. Hence, the ''barotropic governor'' mechanism proposed by LH01 and Yang and Chang (2007) does not seem to contribute to this negative feedback.

In the long term (i.e., beyond a few days), the classical positive synoptic eddy feedback is observed. This feedback clearly occurs for PC1 and is driven by a baroclinic type mechanism: a baroclinicity anomaly, caused by the jet shift, induces an anomaly of the meridional heat flux or source of wave activity, which in turn leads to a convergence of momentum that maintains the jet shift.

In future studies, sensitivity of these different feedbacks to various model parameters (intensity and latitude of the temperature forcing, dissipation coefficients, radii of deformation) will be performed. A particular advantage of the three-level model is that it includes 2 degrees of freedom for the temperature and thus the baroclinicity, which is well suited to analyze climate change effects (Shaw et al. 2016). The identification of the short-term feedbacks of the present study also motivates revisiting the differences between the leading modes of variability in observed jets or in comprehensive GCMs as initiated in Simpson et al. (2013) and Lorenz (2015).

Acknowledgments. The authors thank three anonymous reviewers for their very helpful and insightful remarks.

REFERENCES

Arakelian, A., and F. Codron, 2012: Southern Hemisphere jet variability in the IPSL GCM at varying resolutions. *J. Atmos. Sci.*, **69**, 3788–3799, doi:10.1175/JAS-D-12-0119.1.

Barnes, E. A., and D. L. Hartmann, 2011: Rossby wave scales, propagation, and the variability of eddy-driven jets. *J. Atmos. Sci.*, **68**, 2893–2908, doi:10.1175/JAS-D-11-039.1.

——, and D. W. J. Thompson, 2014: Comparing the roles of barotropic versus baroclinic feedbacks in the atmospheres response to mechanical forcing. *J. Atmos. Sci.*, **71**, 177–194, doi:10.1175/JAS-D-13-070.1.

Codron, F., 2007: Relations between annular modes and the mean state: Southern Hemisphere winter. *J. Atmos. Sci.*, **64**, 3328–3339, doi:10.1175/JAS4012.1.

Eichelberger, S. J., and D. L. Hartmann, 2007: Zonal jet structure and the leading mode of variability. *J. Climate*, **20**, 5149–5163, doi:10.1175/JCLI4279.1.

Feldstein, S. B., and S. Lee, 1996: Mechanisms of zonal index variability in an aquaplanet GCM. *J. Atmos. Sci.*, **53**, 3541–3555, doi:10.1175/1520-0469(1996)053<3541:MOZIVI>2.0.CO;2.

Gerber, E. P., and G. K. Vallis, 2007: Eddy–zonal flow interactions and the persistence of the zonal index. *J. Atmos. Sci.*, **64**, 3296–3311, doi:10.1175/JAS4006.1.

James, I. N., 1987: Suppression of baroclinic instability in horizontally sheared flows. *J. Atmos. Sci.*, **44**, 3710–3720, doi:10.1175/1520-0469(1987)044<3710:SOBIIH>2.0.CO;2.

Linkin, M. E., and S. Nigam, 2008: The North Pacific Oscillation–west Pacific teleconnection pattern: Mature-phase structure and winter impacts. *J. Climate*, **21**, 1979–1997, doi:10.1175/2007JCLI2048.1.

Lorenz, D. J., 2014: Understanding midlatitude jet variability and change using Rossby wave chromatography: Wave–mean flow interaction. *J. Atmos. Sci.*, **71**, 3684–3705, doi:10.1175/JAS-D-13-0201.1.

——, 2015: Understanding midlatitude jet variability and change using Rossby wave chromatography: Methodology. *J. Atmos. Sci.*, **72**, 369–388, doi:10.1175/JAS-D-13-0199.1.

——, and D. L. Hartmann, 2001: Eddy–zonal flow feedback in the Southern Hemisphere. *J. Atmos. Sci.*, **58**, 3312–3327, doi:10.1175/1520-0469(2001)058<3312:EZFFIT>2.0.CO;2.

——, and ——, 2003: Eddy–zonal flow feedback in the Northern Hemisphere winter. *J. Climate*, **16**, 1212–1227, doi:10.1175/1520-0442(2003)16<1212:EFFITN>2.0.CO;2.

Lorenz, E. N., 1955: Available potential energy and the maintenance of the general circulation. *Tellus*, **7**, 157–167, doi:10.3402/tellusa.v7i2.8796.

Marshall, J., and F. Molteni, 1993: Toward a dynamical understanding of planetary-scale flow regimes. *J. Atmos. Sci.*, **50**, 1792–1818, doi:10.1175/1520-0469(1993)050<1792:TADUOP>2.0.CO;2.

Michel, C., and G. Rivière, 2014: Sensitivity of the position and variability of the eddy–driven jet to different SST profiles in an aquaplanet general circulation model. *J. Atmos. Sci.*, **71**, 349–371, doi:10.1175/JAS-D-13-074.1.

Moon, W., and S. B. Feldstein, 2009: Two types of baroclinic life cycles during the Southern Hemisphere summer. *J. Atmos. Sci.*, **66**, 1401–1417, doi:10.1175/2008JAS2826.1.

O'Rourke, A. K., and G. K. Vallis, 2013: Jet interaction and the influence of a minimum phase speed bound on the propagation of eddies. *J. Atmos. Sci.*, **70**, 2614–2628, doi:10.1175/JAS-D-12-0303.1.

——, and ——, 2016: Meridional Rossby wave generation and propagation in the maintenance of the wintertime tropospheric double jet. *J. Atmos. Sci.*, **73**, 2179–2201, doi:10.1175/JAS-D-15-0197.1.

Ring, M. J., and A. R. Plumb, 2008: The response of a simplified GCM to axisymmetric forcings: Applicability of the fluctuation–dissipation theorem. *J. Atmos. Sci.*, **65**, 3880–3898, doi:10.1175/2008JAS2773.1.

Rivière, G., 2009: The effect of latitudinal variations in low-level baroclinicity on eddy life cycles and upper-tropospheric wave-breaking processes. *J. Atmos. Sci.*, **66**, 1569–1592, doi:10.1175/2008JAS2919.1.

——, 2010: Role of Rossby wave breaking in the west Pacific teleconnection. *Geophys. Res. Lett.*, **37**, L11802, doi:10.1029/2010GL043309.

——, J.-B. Gilet, and L. Oruba, 2013: Understanding the regeneration stage undergone by surface cyclones crossing a midlatitude jet in a two-layer model. *J. Atmos. Sci.*, **70**, 2832–2853, doi:10.1175/JAS-D-12-0345.1.

——, L. Robert, and F. Codron, 2016: A short-term negative eddy feedback on midlatitude jet variability due to planetary wave reflections. *J. Atmos. Sci.*, **73**, 4311–4328, doi:10.1175/JAS-D-16-0079.1.

Robinson, W. A., 2000: A baroclinic mechanism for the eddy feedback on the zonal index. *J. Atmos. Sci.*, **57**, 415–422, doi:10.1175/1520-0469(2000)057<0415:ABMFTE>2.0.CO;2.

Shaw, T., and Coauthors, 2016: Storm track processes and the opposing influences of climate change. *Nat. Geosci.*, **9**, 656–664, doi:10.1038/ngeo2783.

Simmons, A. J., and B. J. Hoskins, 1978: The life cycle of some nonlinear baroclinic waves. *J. Atmos. Sci.*, **35**, 414–432, doi:10.1175/1520-0469(1978)035<0414:TLCOSN>2.0.CO;2.

Simpson, I. R., T. G. Shepherd, P. Hitchcock, and J. F. Scinocca, 2013: Southern annular mode dynamics in observations and models. Part II: Eddy feedbacks. *J. Climate*, **26**, 5220–5241, doi:10.1175/JCLI-D-12-00495.1.

Thompson, D. W. J., and J. M. Wallace, 2000: Annular modes in the extratropical circulation. Part I: Month-to-month variability. *J. Climate*, **13**, 1000–1016, doi:10.1175/1520-0442(2000)013<1000:AMITEC>2.0.CO;2.

Vallis, G. K., 2006: *Atmospheric and Oceanic Fluid Dynamics.* Cambridge University Press, 745 pp.

——, and E. P. Gerber, 2008: Local and hemispheric dynamics of the North Atlantic Oscillation, annular patterns and the zonal index. *Dyn. Atmos. Oceans*, **44**, 184–212, doi:10.1016/j.dynatmoce.2007.04.003.

Yang, X., and E. K. M. Chang, 2007: Eddy–zonal flow feedback in the Southern Hemisphere winter and summer. *J. Atmos. Sci.*, **64**, 3091–3112, doi:10.1175/JAS4005.1.

Zhang, Y., X.-Q. Yang, Y. Nie, and G. Chen, 2012: Annular mode–like variation in a multilayer quasigeostrophic model. *J. Atmos. Sci.*, **69**, 2940–2958, doi:10.1175/JAS-D-11-0214.1.

Zurita-Gotor, P., J. Blanco-Fuentes, and E. P. Gerber, 2014: The impact of baroclinic eddy feedback on the persistence of jet variability in the two-layer model. *J. Atmos. Sci.*, **71**, 410–429, doi:10.1175/JAS-D-13-0102.1.